Optimized Design of a Coupled-Inductor Buck Converter, 48 to 12 V, 1 kW, Using Planar Magnetics and GaN-FETs for MHz-Range Operation

Track 6. Vehicle Electrification-related Technologies

***Abstract*—The next generation of automotive vehicles and datacenters requires highly compact and efficient 48 V to 12 V point-of-load converters. This paper investigates the impact of coupling on the electrical properties of 2-phase buck converters operating in triangular current mode to achieve soft-switching. A novel planar inductor geometry with four poles and distributed air-gaps for operation beyond 1 MHz is presented that minimizes copper-losses from external proximity effect. An experimental prototype with 1 kW output achieves an impressive power density of 80 kW/l (1300 W/in³) and a peak efficiency of 96.5%, demonstrating the efficacy of the inductor structure.**

***Index Terms*—coupled inductor, magnetic integration, planar inductor, triangular current mode**

I. Introduction

With a growing power demand, power distribution in both conventional and electric vehicles presents an increasing challenge. Traditionally, $12\,\mathrm{V}$ are used to distribute the power to all auxiliary devices which requires large cable diameters. Recently, many researchers proposed a $48\,\mathrm{V}$ distribution bus to reduce the cost of the wire assembly and/or reduce losses CITE. As most devices are still operating at $12\,\mathrm{V}$, highly compact and efficient point-of-load converters are required. This conversion stage is a critical part of distributed power architectures and its performance has a direct impact on system-level efficiency, thermal design, and spatial constraints.

This motivates the use of wide-bandgap semiconductors which offer lower $R_{ds,on}$ and faster switching speeds compared to traditional Si-devices. By increasing the switching frequency, magnetic components and filters can be shrunk significantly enabling very high power densities. Beyond $500\,\mathrm{kHz}$ hard-switched converters are generally unsuitable due to their large switching losses CITE. A lot of research has been done on resonant converters due to their high efficiency and compact design but those are unsuitable when a regulated output voltage is required over a wide input voltage range CITE.

The two phase coupled-inductor buck converter is a promising topology for these applications.

Blabla

II. Coupled inductor buck converter in TCM

A. Working principle

The topology of the two phase coupled-inductor buck converter is shown in figure 1. By integrating both inductors on the same core, the inductor volume can be shrunk significantly while the modulation remains the same: Both legs are switched $180\,\mathrm{deg}$ out of phase. If the ripple is more than twice the phase current, the leg current becomes negative prior to the rising edge of each leg resulting in a zero voltage switching (ZVS) turn-on of all transistors. Only the small turn-off losses are observed now. This mode is called triangular current mode (TCM) [1].

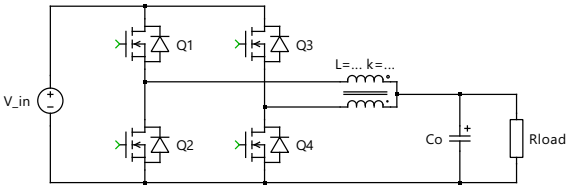

Fig. 1: Schematic of the Coupled Inductor Buck Converter.

B. Impact of the Coupling Factor

The symmetrical coupled inductor consists of two identical coils that are wound in a way, that the flux of one coil links with the flux of the second coil and vice versa with both coils connected on one side. This configuration can be described mathematically using

$$\begin{bmatrix} v_a \\ v_b \end{bmatrix} = \begin{bmatrix} 1 & k \\ k & 1 \end{bmatrix} L_{self} \begin{bmatrix} \frac{di_1}{dt} \\ \frac{di_2}{dt} \end{bmatrix} \tag{1}$$

with self-inductance L_{self} and coupling-factor k. Note that k can be positive or negative; the impact of that will be analyzed later. In order to simplify the equations and provide a more intuitive understanding, the equivalent circuit in figure TODO is introduced. Both circuits are electrically equivalent for

$$\begin{aligned} L_{out} &= (1+k)\frac{L_{self}}{2} \\ L_m &= (1-k)\frac{L_{self}}{2}. \end{aligned} \tag{2}$$

The voltage at the virtual central node is now only dependent of the two leg voltages v_1 and v_2 decoupling the governing

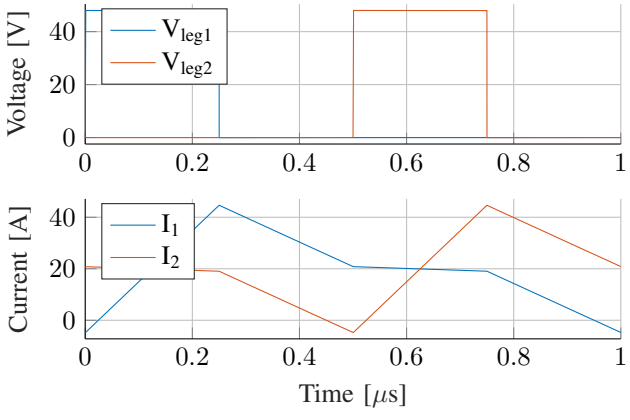

(a) Negative Coupling (k = -0.3)

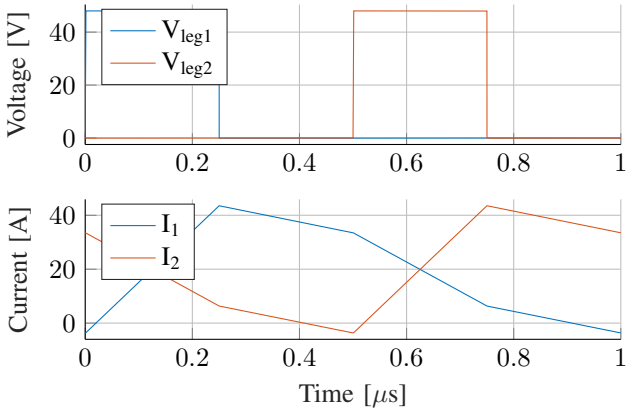

(b) Positive Coupling (k = 0.3)

Fig. 2: Waveforms for positive and negative coupling. It can be seen that the slopes are changed but the behavior in the vicinity of the switching instances is fundamentally the same. ToDo: Make smaller!

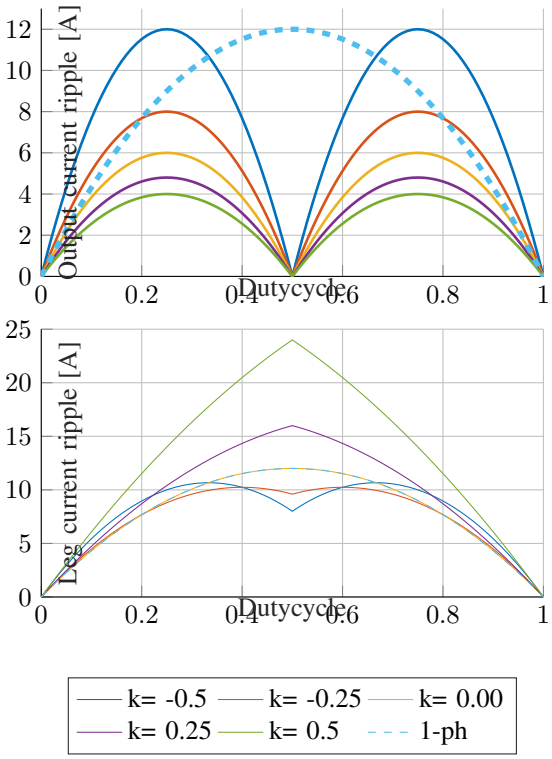

Fig. 3: Output current ripple and leg ripple for different coupling factors and constant input voltage. 1-ph for comparison. ToDo: Redo with normalized y-axis.

equations:

$$\begin{aligned} \frac{di_{out}}{dt} &= \frac{1}{L_{out}}\left(\frac{v_1+v_2}{2} - v_{out}\right) \\ \frac{di_m}{dt} &= \frac{1}{L_{out}}\left(\frac{v_1-v_2}{2}\right) \\ \text{with} \quad i_{out} &= i_1+i_2 \quad \text{and} \quad i_m = i_1-i_2 \end{aligned} \tag{3}$$

From this, the differential equations for each interval can be easily calculated and afterwards the important converter parameters. An effective dutycycle D_{eff} can be introduced with $D_{eff} = D$ for $D \leq 0.5$ and $D_{eff} = 1-D$ for $D > 0.5$. The output ripple is given by

$$\frac{2V_{in}}{f_s(1+k)L_{self}} D_{eff}\left(\frac{1}{2} - D_{eff}\right). \tag{4}$$

The ripple in each leg which is important for soft-switching is

$$\Delta I_{leg} = \frac{V_{in}D_{eff}}{2f_sL_{self}}\left(\frac{2}{1+k}(0.5-D_{eff}) + \frac{1}{1-k}\right). \tag{5}$$

Both are shown in figure 3. There is a strong dependency of these parameters with dutycycle but interestingly, the leg ripple current is not that significantly influenced by the coupling-factor. As the coupling increases, L_{out} increases while L_m decreases causing a decrease in i_{out} but an increase in i_m.

As mentioned before, for soft-switching I_{on} needs to be negative and generally needs to be below a certain value to guarantee a sufficiently short dead time which can be written as $\Delta I_{leg} \geq i_{out} + 2I_{on,max}$. This is fulfilled for

$$f_s < \frac{V_{in}D_{eff}}{2L_{self}(i_{out}+2I_{on,max})}\left(\frac{2}{1+k}(0.5-D_{eff}) + \frac{1}{1-k}\right). \tag{6}$$

III. Inductor Design

A. Inductor geometry

Four different geometries were considered for this application:

- Four-pole structure introduced by [2].

Left: Double-PQ structure [3]. Right: Four-pole structure [2].

B. Material limitations

High-frequency ferrite materials for power applications have some unique properties that differ from those for lower frequency applications. TDK's PC200 was selected for this design as it exhibits very low loss in the range of 1 to 4 MHz. However, the performance of PC200 significantly degrades for a field strength $H_{dc} > 50\,\mathrm{A/m}$ and at $H_{dc} > 100\,\mathrm{A/m}$ its

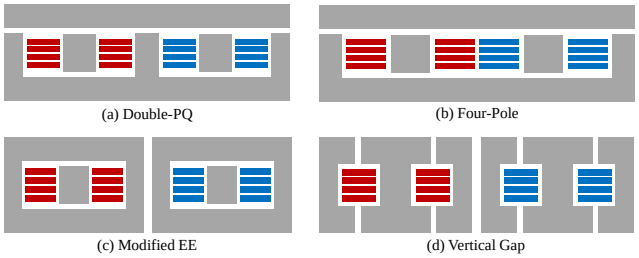

Fig. 4: Structure of the cores; Cut through the center, sie-view. First winding in red, second winding in blue.

losses double [4]. Therefore, the inductor was designed with a maximum H_{dc} of $40\,\mathrm{A/m}$ to have some margin.

IV. Experimental prototype

- Two LS-FETs due to large current. Switching losses don't matter
- Maybe list the key-components: F280049C, LT8418, IGC025S08S1
- Small 0805 capacitors due to resonance
- Incorporates internal vertical layout

A more detailed analysis of the losses will be given in the final paper including a calculated contribution of the dielectric volume loss as introduced by [5].

References

[1] C. Marxgut, J. Biela, and J. W. Kolar, "Interleaved Triangular Current Mode (TCM) resonant transition, single phase PFC rectifier with high efficiency and high power density," in *The 2010 International Power Electronics Conference - ECCE ASIA -*, Jun. 2010, pp. 1725–1732. [Online]. Available: https://ieeexplore.ieee.org/document/5542048

[2] M. Hua, J. Chen, G. Xu, and H. Wu, "Ultra-thin Coupled Inductor for a GaN-Based CRM Buck Converter," in *2021 IEEE Workshop on Wide Bandgap Power Devices and Applications in Asia (WiPDA Asia)*, Aug. 2021, pp. 138–142. [Online]. Available: https://ieeexplore.ieee.org/document/9656036/citations#citations

[3] S. Wang, P. H. Pham, Q. Li, A. Nabih, and P. R. Prakash, "PCB Winding-Based Coupled Inductor for a High-Frequency DC/DC Converter with 99% Efficiency," in *2023 IEEE Applied Power Electronics Conference and Exposition (APEC)*, Mar. 2023, pp. 420–425, iSSN: 2470-6647. [Online]. Available: https://ieeexplore.ieee.org/document/10131439

[4] TDK, "High-Frequency, Low-Loss Ferrite Material PC200." [Online]. Available: https://product.tdk.com/de/techlibrary/productoverview/ferrite_pc200.html

[5] M. Baumann, C. Drexler, J. Pfeiffer, J. Schueltzke, E. Lorenz, and M. Schmidhuber, "Investigation of core-loss mechanisms in large-scale ferrite cores for high-frequency applications," in *2022 24th European Conference on Power Electronics and Applications (EPE'22 ECCE Europe)*, Sep. 2022, pp. 1–10. [Online]. Available: https://ieeexplore.ieee.org/document/9907281